



HAL
open science

Electronic structures of Cu₂O, Cu₄O₃, and CuO: A joint experimental and theoretical study

Yong Wang, Stephan Lany, Jaâfar Ghanbaja, Yannick Fagot-Revurat, Yuan Ping Chen, Flavio Soldera, David Horwat, Frank Mücklich, Jean-François Pierson

► **To cite this version:**

Yong Wang, Stephan Lany, Jaâfar Ghanbaja, Yannick Fagot-Revurat, Yuan Ping Chen, et al.. Electronic structures of Cu₂O, Cu₄O₃, and CuO: A joint experimental and theoretical study. *Physical Review B: Condensed Matter and Materials Physics (1998-2015)*, 2016, 94 (24), pp.245418. 10.1103/PhysRevB.94.245418 . hal-01430765

HAL Id: hal-01430765

<https://hal.science/hal-01430765>

Submitted on 10 Jan 2017

HAL is a multi-disciplinary open access archive for the deposit and dissemination of scientific research documents, whether they are published or not. The documents may come from teaching and research institutions in France or abroad, or from public or private research centers.

L'archive ouverte pluridisciplinaire **HAL**, est destinée au dépôt et à la diffusion de documents scientifiques de niveau recherche, publiés ou non, émanant des établissements d'enseignement et de recherche français ou étrangers, des laboratoires publics ou privés.

Electronic structures of Cu₂O, Cu₄O₃, and CuO: A joint experimental and theoretical studyY. Wang,¹ S. Lany,² J. Ghanbaja,¹ Y. Fagot-Revurat,¹ Y. P. Chen,³ F. Soldera,⁴ D. Horwat,¹ F. Mücklich,⁴ and J. F. Pierson^{1,*}¹*Institut Jean Lamour (UMR CNRS 7198), Université de Lorraine, Nancy 54011, France*²*National Renewable Energy Laboratory, Golden, Colorado 80401, USA*³*Department of Physics, Xiangtan University, Xiangtan 411105, China*⁴*Department for Materials Science, Functional Materials, Saarland University, Saarbrücken D-66123, Germany*

(Received 5 April 2016; revised manuscript received 24 August 2016; published 14 December 2016)

A joint experimental and theoretical study is presented for the electronic structures of copper oxides including Cu₂O, CuO, and the metastable mixed-valence oxide Cu₄O₃. The optical band gap is determined by experimental optical absorption coefficient, and the electronic structure in valence and conduction bands is probed by photoemission and electron energy loss spectroscopies, respectively. The experimental results are compared with many-body *GW* calculations utilizing an additional on-site potential for *d*-orbital energies that facilitates tractable and predictive computations. The side-by-side comparison between the three oxides, including a band insulator (Cu₂O) and two Mott/charge-transfer insulators (CuO, Cu₄O₃) leads to a consistent picture for the optical and band-structure properties of the Cu oxides, strongly supporting indirect band gaps of about 1.2 and 0.8 eV in CuO and Cu₄O₃, respectively. This comparison also points towards surface oxidation and reduction effects that can complicate the interpretation of the photoemission spectra.

DOI: [10.1103/PhysRevB.94.245418](https://doi.org/10.1103/PhysRevB.94.245418)**I. INTRODUCTION**

Cuprous oxide Cu₂O (cuprite) and cupric oxide CuO (tenorite) are important prototypical materials for the electronic structure of oxides. As one of the first known semiconductors, Cu₂O is a band insulator and still of active interest for studying exciton physics [1] and for solar energy conversion, due to the abundance of the elements, nontoxicity, and versatile fabrication routes [2–8]. CuO is described as a strongly correlated charge transfer insulator [9] and serves as a prototype system for high *T_C* superconductors [10]. Cu₂O and CuO have been widely studied for the past three decades, both experimentally [4,9,11–15] and theoretically [4,16–22]. The third oxide phase, Cu₄O₃, is a metastable mixed-valence intermediate compound between Cu₂O and CuO [14,16,23–25] that occurs as the exceedingly rare mineral paramelaconite, giving rise to a mysterious veil.

The band structure of Cu₂O is experimentally well established, with a dipole forbidden direct gap at 2.17 eV and a difference of 0.45 eV between the first (forbidden) and second (allowed) conduction band at the zone center [4,26,27]. Computationally, however, the accurate description of Cu₂O is still challenging. For example, even when different calculations agree in the direct band gap of about 2 eV, there can be discrepancies in the conduction band ordering [16]. Although CuO has received wide attention since the discovery of high temperature cuprate superconductors, its electronic structure has not been fully settled. The onset of direct-allowed absorption has been determined at 1.57 eV at low temperature [15], but the type of band gap (direct [28–30] or indirect [12,16,21,31]) remains controversial. The correlated nature of CuO presents a greater challenge for electronic structure calculations. The local density approximation (LDA) fails to predict both band gap and magnetism in CuO. The

opening of a band gap and the correct antiferromagnetic ground state is obtained in LDA + *U* [31] and with Heyd-Scuseria-Ernzerhof (HSE) hybrid functionals [16]. However, a band gap prediction is not possible with these functionals, since LDA + *U* underestimates the Cu₂O gap (0.99 vs 2.17 eV), and hybrid functionals overestimate the CuO gap (2.74 vs 1.57 eV direct) [16]. A recent *GW* study demonstrated that the band gap energy and density of states (DOS) in CuO strongly depend on rather subtle details of the calculations [21]. The current knowledge about the electronic structure of Cu₄O₃ is even more limited. From optical absorption in thin films, the band gap was estimated between 1.3 and 2.5 eV, depending on whether a direct or indirect gap was assumed for the analysis [14]. Calculations using LDA + *U* and HSE hybrid functionals have been employed to calculate the electronic structure of Cu₄O₃ [16,24], but these results are subject to the same ambiguities as mentioned above for CuO.

In view of the interest in Cu oxides as solar energy conversion materials [4,8], it is highly desirable to fill the knowledge gaps that still exist in particular for the Cu²⁺ containing oxides. Hence, the aim of this joint experimental and theoretical study is to develop a comprehensive electronic structure picture across all three Cu oxides. Experimentally, we characterize thin film samples of Cu₂O, CuO, and Cu₄O₃. Photoemission spectroscopy with different photon energies is used to determine the valence band electronic structure. The optical properties are determined from optical absorption coefficient measurements by a spectrophotometry, which allows more direct access to the band gap energies than other optical methods, e.g., ellipsometry, especially in the presence of subgap absorption. For the conduction band structure, we employ electron energy loss spectroscopy (EELS), which has rapidly grown as a useful technique to study the unoccupied electronic states, with great advantages due to large penetration depth and high spatial resolution. In EELS measurements, electrons are excited from core states into unoccupied states [32], allowing the comparison with the calculated

*jean-francois.pierson@univ-lorraine.fr

conduction band DOS under consideration of dipole selection rules.

Computationally, many-body perturbation theory in the GW approximation has emerged as a standard computational tool to predict the electronic structures of semiconductors and insulators, yielding systematic improvements with respect to other methods [17,18,33–35]. Although various GW schemes have been introduced and tested for transition metal (TM) oxides, a single universal scheme that can describe the band structures reliably for a wide range of TM oxides is not yet available. Recently, a GW scheme with local-field effects and an empirical on-site potential (V_d) for TM d orbitals has been proposed, which allows for reasonably predictive band gaps for different oxide stoichiometries and TM oxidation states at an acceptable computational expense [17,36]. However, the band gap is just one characteristic of electronic structure of semiconductors or insulators and does not contain detailed information on the electronic structure as a whole. Thus, we here present a side-by-side comparison of the full optical absorption spectrum and of the quasiparticle DOS in both the valence and conduction band.

II. EXPERIMENTAL AND COMPUTATIONAL DETAILS

A. Experiments

Cu_2O , Cu_4O_3 , and CuO thin films were deposited on glass and (100) silicon substrates at room temperature by reactive pulsed-DC magnetron sputtering in an argon and oxygen atmosphere. The Ar flow rate was fixed at 25 sccm, while the O_2 flow rate was 13, 19, and 24 sccm for single phase Cu_2O , Cu_4O_3 , and CuO , respectively. X-ray diffraction and micro-Raman spectrometry were used to check the phase structures. More details concerning the thin film growth and the characterization can be found in Refs. [23] and [37].

The p -type conductivity of Cu_2O thin film has been identified by Hall effect measurements in a previous paper [38]. Here, positive Seebeck coefficients of Cu_4O_3 ($+102 \mu\text{V}/\text{K}$) and CuO ($+180 \mu\text{V}/\text{K}$) thin films have been attained, indicating p -type conductivity. The optical absorption coefficient at room temperature was determined from transmission (T) and reflectance (R) spectra measured by an ultraviolet-visible-near infrared (UV-Vis-NIR) spectrophotometry (Varian Cary 5000).

The photoemission spectra were measured in an ultrahigh vacuum (UHV) experimental setup equipped with a photoemission analyzer (Scienta SES-200). Al $K\alpha$ (1486.7 eV) and He I (21.2 eV) photon sources were employed for x-ray photoemission spectroscopy (XPS) and ultraviolet photoemission spectroscopy (UPS) measurements, respectively. The Ar^+ ion etching was performed to clean the surface until there is no evolution in the C-1s XPS core level spectra. Silver paste was put in the corner of samples, contacting with the metallic holder. The purpose of this is to relieve the charge effect during the measurement and to identify the Fermi level by using silver as a reference.

The EELS experiments were carried out in a transmission electron microscopy (JEOL ARM 200-Cold FEG fitted with a GIF Quantum ER) equipped with an EELS spectrometer. For the acquisition of energy loss near edge structure (ELNES)

spectra, an accelerating voltage of 200 kV, an emission current of $5 \mu\text{A}$ and an energy dispersion of 0.05 eV/ch were employed. All the spectra were recorded in the image mode, with the energy resolution of $0.45 \sim 0.5$ eV defined by the full width at half maximum (FWHM) of the zero loss peak (ZLP). The convergence semiangle α and the collection semiangle β were 7 and 18 mrad, respectively. Before the EELS spectra measurements, the cross-sectional thin foils were prepared by a focused ion beam (FIB) scanning electron microscope (SEM) dual beam system (FEI Helios 600) using the *in situ* liftout technique. The FIB thinning was performed at high energy (30 keV) followed by a cleaning step at low energy (5 keV) to minimize surface amorphization effects and ion implantation.

B. Calculations

The electronic structures of Cu_2O , Cu_4O_3 , and CuO were calculated within the GW method [39], employing the projector augmented wave (PAW) implementation for density functional theory (DFT) and GW calculations in the Vienna *Ab initio* Simulation Package (VASP) code [40,41]. For monoclinic CuO , the experimentally known low temperature antiferromagnetic configuration [42] with a 16 atom unit cell was used. In paramelaconite Cu_4O_3 , the 14 atom primitive cell has four nonmagnetic Cu^{1+} and four magnetic Cu^{2+} ions, and we used the lowest energy antiferromagnetic configuration within this cell, as given in the generalized gradient approximation (GGA) [43] with a Coulomb parameter of $U = 5$ eV [44] for Cu - d orbitals. As described in detail in Refs. [17] and [36], the present GW scheme was defined such to allow fairly efficient calculations over a wide range of materials using a uniform approach. Specifically, after an initial GGA + U calculation, the wave functions are kept constant, and the GW quasiparticle energies are iterated to self-consistency, using the random phase approximation (RPA) for W . Density functional theory derived local field (LF) effects are included via time-dependent DFT (TD-DFT) [45], which increases somewhat the dielectric response and consequently yields smaller band gaps compared to the random phase approximation. Using an energy cutoff of 330 eV and a total number of bands of $64 * n_{\text{at}}$, where n_{at} is the number of atoms in the unit cell, this approach yields fairly accurate band gaps for main group compounds, typically with less than 10% deviation from experiment.

However, following this approach, the d -orbitals are systematically located at too high energies in the case of $3d$ oxides [17], which is likely the combined result due to several limitations, i.e., the slow convergence behavior of d -orbital energies with respect to the number of bands [46], omission of vertex corrections [47,48], and spurious hybridization effects in the DFT + U wave functions [49]. Rather than resorting to computationally more demanding approaches, this issue was addressed in the $GW^{\text{LF}} + V_d$ approach [17] by an additional on-site potential V_d , which acts to lower the d -orbitals energies, thereby placing them at the correct energy relative to the spectrum of sp states. The potential strength parameter was determined in Ref. [17] empirically by comparison with experimental data for the $3d$ oxides. For example, $V_d = -2.4$ eV was found for Cu - d based on data for Cu_2O and CuO . Even though the V_d parameter is of empirical nature, we found that it is fairly system independent, thereby

allowing real predictions for materials whose band gaps and optical properties are unknown. We further emphasize that V_d is simply a constant potential offset for the average d -orbital energy and does not directly affect electron correlation. All electron-electron correlation effects are handled by the GW method. Note that these present GW calculations are part of a larger dataset of electronic structure calculations for semiconductors and insulators, including TM compounds [36], which is accessible at <http://materials.nrel.gov>.

For the purpose of this paper, we use GW quasiparticle energy spectrum, which omits lifetime broadening effects and satellite structures. A more detailed analysis of these effects is in principle possible within the GW approach, but lies beyond the scope of this paper which focuses on the comparison between the different Cu oxides. Considering the different photoionization cross-sections for O- p and Cu- d states in UPS and XPS (see below), we determined the angular-momentum resolved partial DOS (PDOS), using an integration radius of 1.0 Å, so to facilitate the comparison with experiment. A Gaussian broadening with a width of 0.4 eV was used for comparison with the experimental spectra. Similarly, the PDOS is also used for the comparison with EELS spectra, where the transition matrix elements for the photoionization are rudimentarily accounted for by selecting the angular momentum for the PDOS according to the dipole selection rules. We also note that the electron-core hole interaction is not explicitly taken into account, i.e., the alignment of the computational and experimental spectra implies a rigid shift of the DOS due to the core hole effect. Explicit core-hole calculations can be done in supercell calculations in all-electron approaches, or by using the so-called $Z + 1$ approximation or core-hole pseudopotentials [50]. However, such supercell calculations usually require a more approximate DFT functional. Thus, an alignment is generally still needed, and the underestimated band gaps and band widths in DFT need to be corrected for [50]. By taking the results of GW calculations for the experiment-theory comparison, this paper aims to provide a better description of the conduction band quasiparticle energies but, on the other hand, relies on a rather basic model for simulating the spectra.

The optical absorption spectra are calculated in two different approximations, i.e., the independent particle approximation (IPA), and including excitonic effects within TD-DFT using a hybrid-functional kernel [45]. Here, we used a distance-independent fraction of $1/\epsilon$ of the Hartree-Fock (HF) exchange, where ϵ is the static electronic dielectric constant obtained from the preceding GW calculation. These results are labeled “TD-HF” in the following. For better comparability, the k -derivatives of the wave functions were calculated using a finite differences approach [51] for either of the two approximations. The calculated TD-HF spectra are subject to a Lorentzian broadening of 50 meV width.

III. RESULTS AND DISCUSSIONS

A. Thermodynamic properties

Due to the intermediate stoichiometry of Cu₄O₃ between Cu₂O and CuO, it is interesting to investigate their thermodynamic properties. Several attempts have been made for this

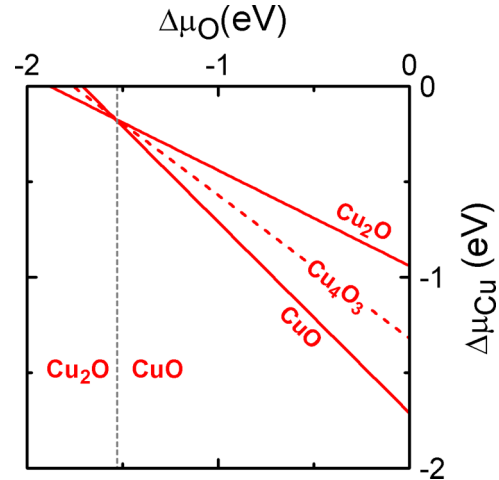


FIG. 1. Phase stability as a function of oxygen chemical potential ($\Delta\mu_O$).

purpose [16,52]. The experimental thermodynamic analysis performed by Blobaum *et al.* [52] shows that Cu₄O₃ is a metastable phase with an upper stability limit that ranges between 670 and 800 K, above which it will decompose into Cu₂O and CuO according to the reaction



Using the total energies calculated in GGA + U and the elemental reference energies of Ref. [53], we show in Fig. 1, the phase stability as a function of the oxygen chemical potential. The transition between CuO and Cu₂O lies at $\Delta\mu_O = -1.53$ eV, close to the transition point at -1.51 eV obtained from tabulated experimental formation enthalpies of CuO and Cu₂O. In the vicinity of this phase transition, Cu₄O₃ is very close in free energy to Cu₂O and CuO. The decomposition energy of Cu₄O₃ according to Eq. (1) is found to be only 17 meV per formula unit (2 meV/atom). Such a small energy indicates a weak thermodynamic driving force for the decomposition of Cu₄O₃. These results are qualitatively similar to the HSE calculations of Heinemann *et al.* [16], although the decomposition energy seems to be significantly larger in HSE. Experimentally, we observe that the thermal stability of Cu₄O₃ in air is close to that of Cu₂O, indicating similar kinetic barriers for the oxidation towards CuO which is the thermodynamic ground state in air ($p_{\text{O}_2} = 0.2$ atm) up to about 1000 °C.

B. Band gap

The band gap and optical properties of Cu₂O have already been widely studied in theoretical calculations and experiments [4,14,16,18,35,54]. Experimentally, it is well established that Cu₂O has a direct forbidden gap of about 2.17 eV and a direct optically allowed band gap of 2.62 eV (low temperature values). The results of the present GW calculations and thin film room temperature measurements for Cu₂O, Cu₄O₃, and CuO are summarized in Table I, showing good overall consistency for all three oxides. For Cu₂O, it should be noted that this GW approach yields the correct conduction band ordering with a difference of

TABLE I. The band gap energies (in eV) of Cu_2O , Cu_4O_3 , and CuO obtained from the GW calculations and experiments. The direct (d) or indirect (i) nature of the gap (E_g) has been noted. (E_{abs}) is the absorption threshold energy for direct and allowed optical transitions (in the IPA), determined somewhat arbitrarily from $\alpha > 10^3 \text{ cm}^{-1}$. (E_{abs}^*) is the experimental optical absorption threshold energy, which is identified from the inflection point.

	GW calculation		Experiment
	(E_g)	(E_{abs})	(E_{abs}^*)
Cu_2O	2.04 (d)	2.53	2.5 ^a
Cu_4O_3	0.84 (i)	1.61	1.37
CuO	1.24 (i)	1.48	1.44

^aReference [38].

$\Delta E_C = +0.66 \text{ eV}$ between the allowed and the forbidden transition at Γ [17], slightly larger than the experimental value of $+0.45 \text{ eV}$ [4,26,27]. Without the onsite potential, the band ordering is inverted, even when a HSE hybrid functional is used as the starting point [17].

Figure 2(a) shows the experimental and calculated absorption coefficients α of Cu_4O_3 . The GW calculation predicts an indirect band gap of 0.84 eV and a direct band gap of 1.59 eV with an absorption onset of 1.61 eV in the IPA (see Fig. 2(a) and Table I), just above the direct gap. It should be pointed out that the calculations do not include phonon-assisted indirect transitions and are performed for the low temperature antiferromagnetic configuration, whereas magnetic fluctuations above the Neel temperature could affect the optical absorption in the experimental measurement. As seen in Fig. 2(a), the experimental optical absorption spectrum shows two regions, as indicated by the green dash lines. At photon energies larger than 1.37 eV , the absorption coefficient increases sharply with increasing photon energy. The tail below 1.37 eV is subject to the subgap absorption, and the oscillation is ascribed to the interference effect.

The origin of two absorption regions in experimental spectrum of Cu_4O_3 thin films could come from a variety of

factors. One possible source is the phonon assisted transitions with low intensity. As the indirect band gap of 0.84 eV predicted by the GW calculation is much lower than the direct band transition of 1.59 eV , the phonon assisted transitions at room temperature may cause absorption below the direct gap. Excitonic effects corresponding to the excitation of delocalized electron-hole pairs also contribute to the subgap absorption. As shown in Fig. 2(a), the excitonic effects in the TD-HF calculation cause a redshift of about 150 meV compared to the IPA. Other intra-atomic $d-d$ and/or $s-d$ excitations could also produce subgap absorption in TM oxides, although they have not been reported in binary copper oxides. Yet another source of subgap absorption could be defect states. In Cu_2O , a defect band tail has been clearly identified by the analysis of subgap absorption [38], which is also detected in the present UPS spectrum with the nonzero states close to Fermi level (see the Supplemental Material [55]). However, such nonzero states are not noticeable in Cu_4O_3 and CuO thin films, indicating that valence band tails are less prevalent in these materials. On the other hand, the large estimated Urbach energy of 0.77 eV (equal to 56% of the optical absorption threshold energy) seems to be inconsistent with the high degree of crystallinity of the Cu_4O_3 thin films (see Ref. [23]), thus speaking against subgap absorption due to defect band tails. While the different mechanisms may jointly contribute to the absorption below the direct gap, the spectra are consistent with the picture given by the present GW calculations. Thus, the observation of an absorption tail corroborates the prediction of an indirect band gap.

Previous HSE calculations gave a much larger band gap of Cu_4O_3 at 2.5 eV and also showed a significant overestimation for CuO [16]. These discrepancies for the Cu^{2+} containing oxides are surprising, since the HSE functional gives a very accurate description of the Cu^{1+} oxide Cu_2O [16,17]. Even when considering that the appropriate fraction of Fock exchange (fixed at $\alpha = 0.25$ in HSE) should decrease with increasing dielectric screening, the observed trends of HSE band gaps are hard to reconcile, as the dielectric constants vary only little between the three oxides. From our present GW calculations, we obtain electronic static dielectric constants

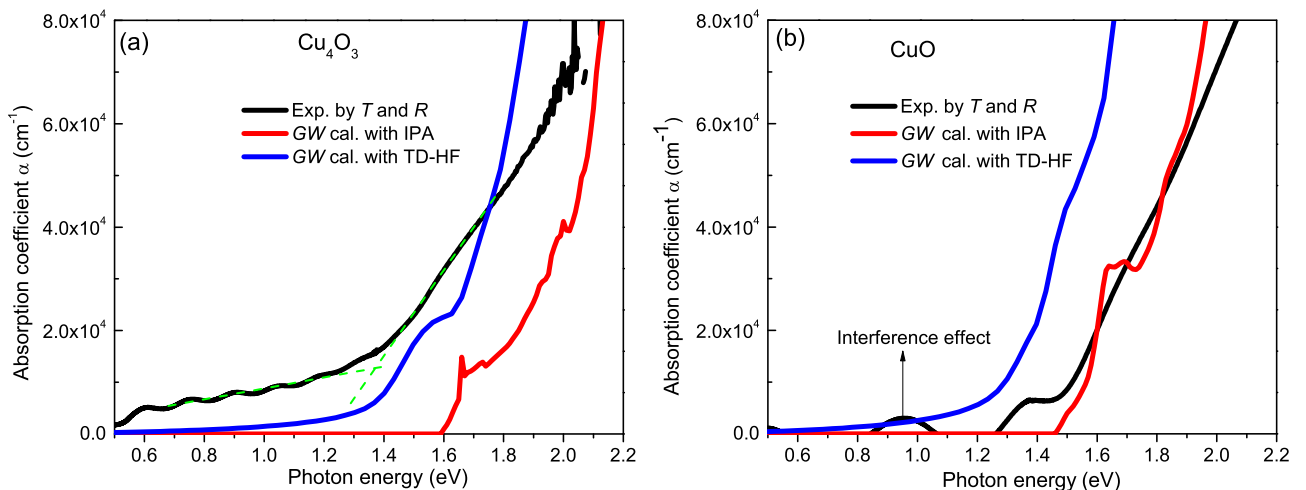


FIG. 2. (a) Experimental and calculated absorption coefficients of Cu_4O_3 . The green dashed lines show two regions with different slopes of the absorption coefficient as a function of the photon energy. (b) Experimental and calculated absorption coefficients of CuO .

of $\varepsilon = 5.7$, 6.2 , and 7.1 for Cu_2O , Cu_4O_3 , and CuO . Thus, as a signature of electron correlation in Cu^{2+} oxides, the magnitude of the band gap seems to be affected by dynamic (energy dependent) or nonlocal screening effects within the $\text{Cu}-d^9$ manifold, which are included in GW , but not in the HSE Hamiltonian.

Moving on to CuO , the experimental and calculated absorption coefficient spectra are shown in Fig. 2(b). An indirect band gap of 1.24 eV and a direct band gap of 1.46 eV are predicted by the GW calculation (see Table I). As seen in Fig. 2(b), the experimental absorption of the CuO thin film also shows two different regions: the absorption rises fast when the photon energy is over 1.44 eV; the absorption at photon energy between 1.3 and 1.44 eV is weak, but quite clear, even when considering the interference effect. Such absorption below the direct gap has also been observed in single crystal CuO between 10 and 300 K [15]. The experimental absorption onset energy of about 1.44 eV at room temperature here agrees well with the theoretical value of 1.46 eV, as well as the onset at 1.34 eV in the single crystals at 300 K [15]. The same mechanisms for a slow absorption onset as discussed above for Cu_4O_3 apply here as well. For instance, the excitonic effects calculated by TD-HF theory cause a similar redshift, as shown in Fig. 2(b). The difference between the calculated indirect and direct band gaps is much smaller in CuO than in Cu_4O_3 , which could explain the fact that the low energy tail in the absorption spectrum of Cu_4O_3 is more pronounced than in CuO . This observation again supports the presence of an indirect gap.

Similar to the case of Cu_4O_3 , previous HSE calculations for CuO also showed a large overestimation of the band

gap [16]. A recent paper comparing different GW schemes noted the extreme sensitivity of the band gap depending on the starting point and degree of self-consistency [21]. While details of electronic screening and subtle differences in the electronic wave functions evidently play an important role, the physical origin of these variations is not well understood. From a practical perspective, the current GW results provide a consistent description between Cu_2O , Cu_4O_3 , and CuO , but it is also clear that these materials will remain crucial test cases for future developments in electronic structure theory.

C. Valence band electronic structure

The valence band electronic structure has been investigated by XPS and UPS and is compared with the calculated DOS. Before discussing the results in detail, we briefly comment on the relative sensitivities of the two photoemission sources on the $\text{O}-2p$ and $\text{Cu}-3d$ spectral weights. $\text{Al K}\alpha$ (1486.7 eV) and He I (21.2 eV) sources have been employed to record the valence band spectra for XPS and UPS, respectively. The cross-section ratios of $\sigma(\text{O}-2p)/\sigma(\text{Cu}-3d) \approx 0.02$ and 1.41 for $\text{Al K}\alpha$ and He I , respectively, are determined utilizing the known energy dependence of the photoionization cross-section [56]. This means that XPS primarily probes the d states, whereas $\text{O}-p$ states are excited with higher, albeit comparable, probability than and the $\text{Cu}-d$ states in UPS. It is also important to note that UPS is more surface sensitive than XPS and thus very sensitive to surface contamination and surface oxidation or reduction processes.

The photoemission valence band spectra and the theoretical DOS of Cu_2O are shown in Fig. 3(a), where the valence

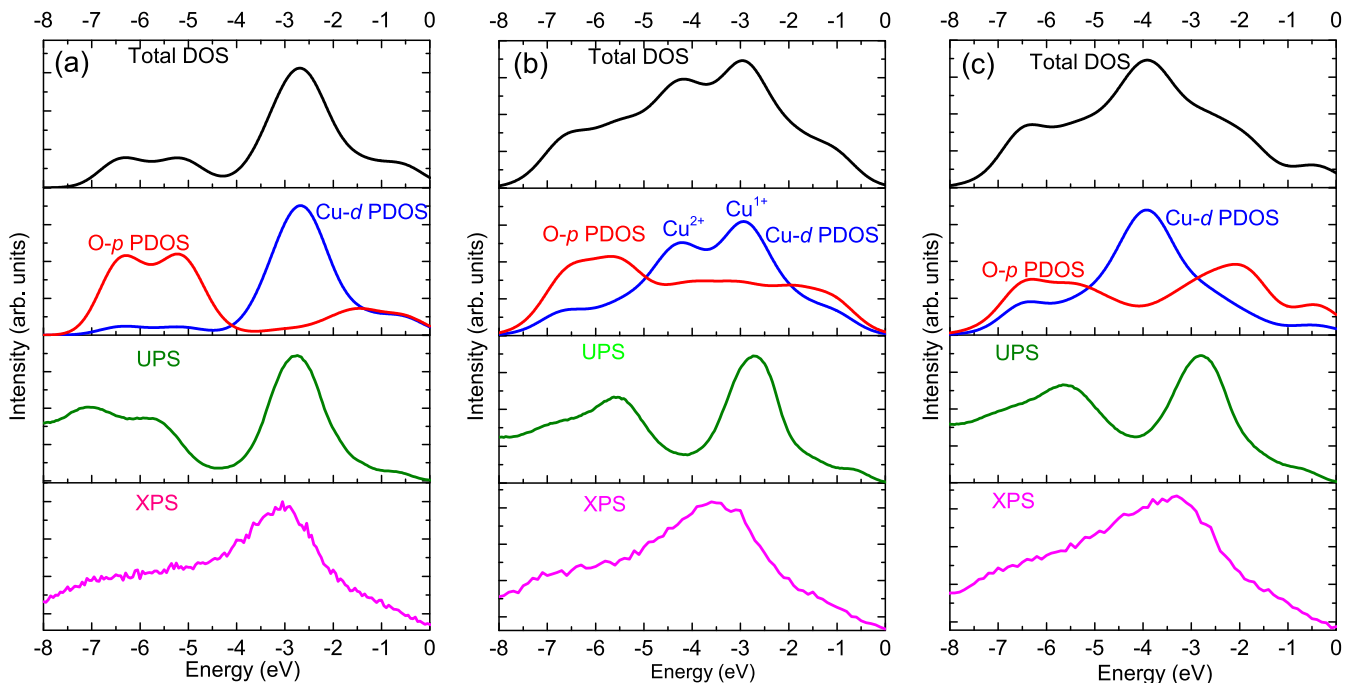


FIG. 3. Experimental valence band spectra and theoretical DOS for (a) Cu_2O , (b) Cu_4O_3 , and (c) CuO . The VBM is set to zero. The theoretical total DOS (in black), $\text{O}-p$ (in red) and $\text{Cu}-d$ (in blue) PDOS are convoluted with a Gaussian broadening of 0.4 eV to mimic extrinsic broadening effects. All theoretical DOS have been normalized to integrate to unity over the valence band. The UPS and XPS spectra are plotted in green and magenta, respectively.

band maximum (VBM) is set to zero. One can distinguish three energy regions in the theoretical DOS. Between -8 and -4 eV, it is dominated by O-2*p* character. Pronounced Cu-3*d* states are concentrated in the energy range of -4 to -1.5 eV with a peak at -2.7 eV. Due to hybridization, the states close to the VBM (-1.5 to 0 eV) have both Cu-3*d* and O-2*p* character with similar intensities. As shown in Fig. 3(a), the UPS spectrum is consistent with the calculated DOS when considering the contributions from both O-2*p* and Cu-3*d*. As expected, the XPS spectrum shows mainly the Cu-3*d* contributions, and the features due to the O-2*p* states are less pronounced. Looking at the dominant O-2*p* character in the energy range of -8 to -4 eV, the theoretical DOS exhibit similar shape with respect to UPS spectrum, but the theoretical peak positions are shifted approximately 0.6 eV to higher energies. This discrepancy indicates that the present *GW* calculations underestimate somewhat the valence band width. Notably, HSE calculations [16,17] reproduce the energies of the O-2*p* related peaks between -8 and -5 eV almost perfectly, notwithstanding the above discussed issues related to the band gaps of the Cu²⁺ containing oxides.

Figure 3(b) compares the photoemission spectra and theoretical DOS for the metastable mixed-valence phase Cu₄O₃. The O-2*p* PDOS stretches over the entire valence band energy range but has an increased intensity between -7 and -5 eV, which is also reflected in the UPS spectrum. The Cu-3*d* PDOS has a double-peak structure with maxima at -2.9 and -4.3 eV, corresponding to Cu¹⁺ and Cu²⁺ sites, respectively. The larger binding energy of the Cu²⁺ sites can be understood by the reduction of the Coulomb repulsion in the *d*⁹ configuration as compared to the *d*¹⁰ configuration of Cu¹⁺, thereby indicating correlation effects. The UPS spectrum shows a peak at -2.7 eV, in good agreement with the calculated peak position due to Cu¹⁺, but the expected lower energy signal for Cu²⁺ is not observed. Indeed, the UPS spectrum shows a valley in the energy range around -4 eV. Note that the calculated PDOS due to O-2*p* is practically constant in this energy range and should not affect the peak position measured by UPS. In the XPS spectrum, however, we observe peak shift to lower energies at about -3.5 eV, which agrees reasonably well with the average of the calculated Cu¹⁺ and Cu²⁺ peaks. The absence of the Cu²⁺ peak expected from theory and the pronounced shift of the peak position between UPS and XPS (which is hard to explain by the O-*p* contribution in UPS) could indicate that the surface near the region probed by UPS is a more reduced Cu oxide phase compared to the Cu₄O₃ bulk. The deeper probing depth of XPS picks up the contributions from both oxidation states of Cu, leading to a broadening and shift of the apparent peak energy. Such surface reduction effects seem also to be present in CuO and are likely related to the vacuum instabilities observed in previous photoemission studies [57], as discussed below.

Moving on to monoclinic CuO, we first compare our experimental valence band spectra for CuO thin-films with previously reported experimental results (see the Supplemental Material [55]), demonstrating the consistency with literature data. In Fig. 3(c), the experimental CuO valence band spectra are shown in comparison to the calculated DOS. The O-2*p* DOS shows up in the low energy range between -7 and -5 eV, similar to the case of Cu₂O and Cu₄O₃, but now also dominates

the energies close to the VBM. This behavior can be expected because increasing the Cu oxidation state from $+1$ (*d*¹⁰) to $+2$ (*d*⁹) lowers the *d*-orbital energy due to reduced Coulomb repulsion, so that the O-2*p* intensities dominate at the higher energies. The Cu-3*d* DOS exhibits a single peak structure with a maximum at about 4 eV below the VBM. Since the Cu-3*d* peak is straddled by O-2*p* contributions at both higher and lower energies, CuO cannot unambiguously be labeled as Mott or charge transfer insulator.

It is notable that the Cu-3*d* peak positions occur rather consistently around -3 and -4 eV for Cu¹⁺ and Cu²⁺, respectively, across all three oxides. At first glance, however, the UPS spectrum for CuO seems to be inconsistent with the calculated DOS. The peaks at -2.8 and -5.5 eV roughly resemble the structure of the O-2*p* DOS, but the UPS shows a valley at -4 eV, i.e., at the energy where the calculations place the Cu-3*d* peak. Even when considering the slightly larger UPS cross-section for O-2*p* than for Cu-3*d*, this discrepancy is difficult to reconcile. However, in the XPS spectrum with more Cu 3*d* sensitivity and larger penetration depth than UPS, the peak shifts to about -3.5 eV closer to the predicted Cu-3*d* maximum. The peak at about -3 eV in the UPS spectrum of CuO has also been observed by Thuler *et al.* [58] and Shen *et al.* [57]. However, Shen *et al.* also observed a sideband feature at -4 eV, which disappeared after exposure to vacuum and which was speculated to be due to nonbonding oxygen states. However, in light of the present UPS and XPS measurements for both Cu₄O₃ and CuO and the respective *GW* calculations, it seems likely that the UPS spectra largely correspond to a reduced Cu₂O-like surface phase and that the XPS spectra represent a superposition of intensities from near-surface Cu¹⁺ ions and from Cu²⁺ ions located in the actual Cu₄O₃ and CuO phases. This interpretation would also explain the strong similarities of both UPS and XPS between Cu₄O₃ and CuO [cf. Figs. 3(b) and 3(c)], despite the clearly different characteristics in the conduction band DOS as observed by EELS (see below), which has a much larger probing depth.

D. XPS core level and EELS spectra

The Cu 2*p*_{3/2} XPS core level spectra of copper oxides are shown in Fig. 4. Satellite peaks in CuO due to the intraatomic multiplet coupling and hybridization have been clearly observed, but they are absent in Cu₂O, which agrees with the well-known characteristics of Cu₂O and CuO [9]. Similar satellite peaks in Cu₄O₃ demonstrate the configuration of Cu²⁺ in the ground state. The FWHMs of the main peaks at about 933 eV are 1.7, 1.9, and 2.3 eV in Cu₂O, Cu₄O₃, and CuO, respectively. Due to the similar peak shapes and peak positions, the Cu 2*p*_{3/2} XPS core level spectra do not allow us to further resolve differences between the Cu oxides.

In order to further study the electronic structure of the Cu oxides, we therefore employed EELS. The ELNES spectra of Cu *L*_{2,3} and O *K* edges are shown in Figs. 5(a) and 5(b), respectively. The spectral shape and the relative position of the Cu *L*_{2,3} edges in CuO and Cu₂O are in excellent agreement with previous reports of x-ray absorption spectroscopy (XAS) [13,22,59], including the substructures indicated by asterisks in Fig. 5 in Cu₂O. As seen in Fig. 5(a), strong and

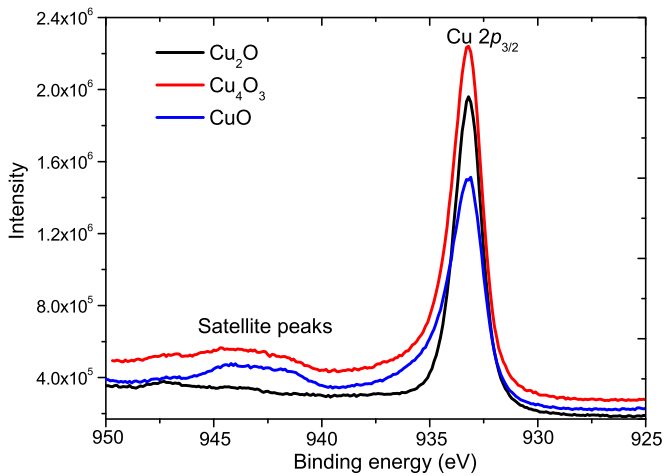


FIG. 4. Cu $2p_{3/2}$ core-level XPS spectra of Cu₂O, Cu₄O₃, and CuO thin films.

sharp $L_{2,3}$ white lines have been clearly observed in Cu₂O, which is in contrast to the traditional simple ionic model. The dipole selection rules allow transitions from the $2p$ level into final states of s ($\Delta l = -1$) or d ($\Delta l = +1$) character, but the $\Delta l = -1$ channel is extremely low, and it can be safely ignored in a first approximation [11]. Hence, the presence of L edges white lines in EELS or XAS requires empty d orbitals, which should be absent in the ionic model for Cu¹⁺ with a closed $3d^{10}$ shell. However, there is quite a strong consensus that the sharp Cu $L_{2,3}$ white lines in Cu₂O can always be measured by EELS or XAS [11,13,22,59]. The origin of this kind of unfilled $3d$ shell in Cu₂O remains controversial. One hypothesis assumes that the $3d$ shell of metallic Cu just contains 9.6 electrons, and there are only 9.5 electrons in the $3d$ orbital of Cu₂O [60,61]. Since this assumption employs the questionable white lines in metallic Cu, we believe that this hypothesis may require careful reconsideration. Another explanation could be the pronounced onsite Cu $3d$ - $4s$ hybridization, which is allowed by symmetry in Cu₂O, will produce a significant intensity of unoccupied d_z^2 states in the conduction band [17], thereby providing a channel for excitation of Cu- $2p$ core level electrons.

Checking the peak positions of Cu $L_{2,3}$ white lines in Cu₂O and CuO [see Fig. 5(a)], it is revealed that the positions of Cu $L_{2,3}$ edges are shifted to lower energy loss for the higher oxidation state. This contradicts the trends in Mn, V, and Fe oxides, in which the energy loss moves to higher energy for the higher oxidation state [62]. Employing the Cu L_3 edges of Cu₂O and CuO as references, the white lines of Cu₄O₃ can be identified easily, where the strongest peak with the energy loss of 931.1 eV corresponds to Cu²⁺, and the peak at 933.7 eV corresponds to Cu¹⁺, as shown in Fig. 5(a). A similar structure exists at the L_2 edge. Concerning the O K edges, these three phases also exhibit significant differences, as shown in Fig. 5(b). Cu₂O shows a prominent peak at 532.5 eV and minor features at higher energy loss. In Cu₄O₃, four energy loss peaks are found at energies of 530.5, 533.4, 536, and 541 eV, whereas in CuO, there are features at 528.4, 532.9, 537.4, and 541 eV. These ELNES features distinguish the different Cu oxide phases more clearly than the XPS and UPS spectra discussed above.

E. Conduction band electronic structure

The L_3 edge in ELNES corresponds to $2p_{3/2}$ electrons being excited into unoccupied d states above Fermi level, while O K edge represents $1s$ electrons being excited into empty p states, within the consideration of the parities of the initial and final states. Thus, it is interesting to compare the experimental Cu L_3 ELNES spectrum with the calculated Cu- d PDOS in the conduction band and, similarly, the O K edge spectra with the O- p PDOS. Figures 6(a) and 6(b) show that the GW calculated unoccupied Cu- d and O- p PDOS match well the basic shape of the respective experimental Cu L_3 and O K ELNES spectra in Cu₂O. The ELNES spectra in Cu₄O₃ exhibit a much richer structure and more features both in the Cu L_3 and O K spectra, which is related to the coexistence of Cu¹⁺ and Cu²⁺ states. Given the simplicity of the approach to compare the experimental spectra with the PDOS (see discussion above), the computational results describe the measured features remarkably well. For example, the two peaks in the Cu L_3 spectrum [Fig. 6(c)] around 1 and 4 eV can be clearly ascribed due to Cu²⁺ and Cu¹⁺ sites in

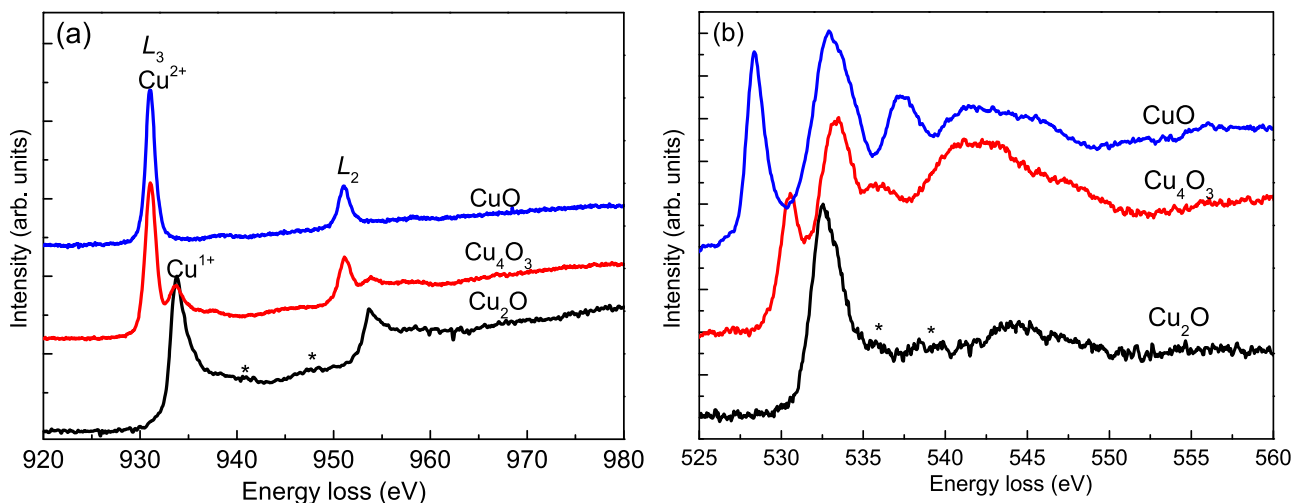


FIG. 5. (a) Cu $L_{2,3}$ edges and (b) O K edge ELNES spectra of Cu₂O, Cu₄O₃, and CuO, normalized to the peak height.

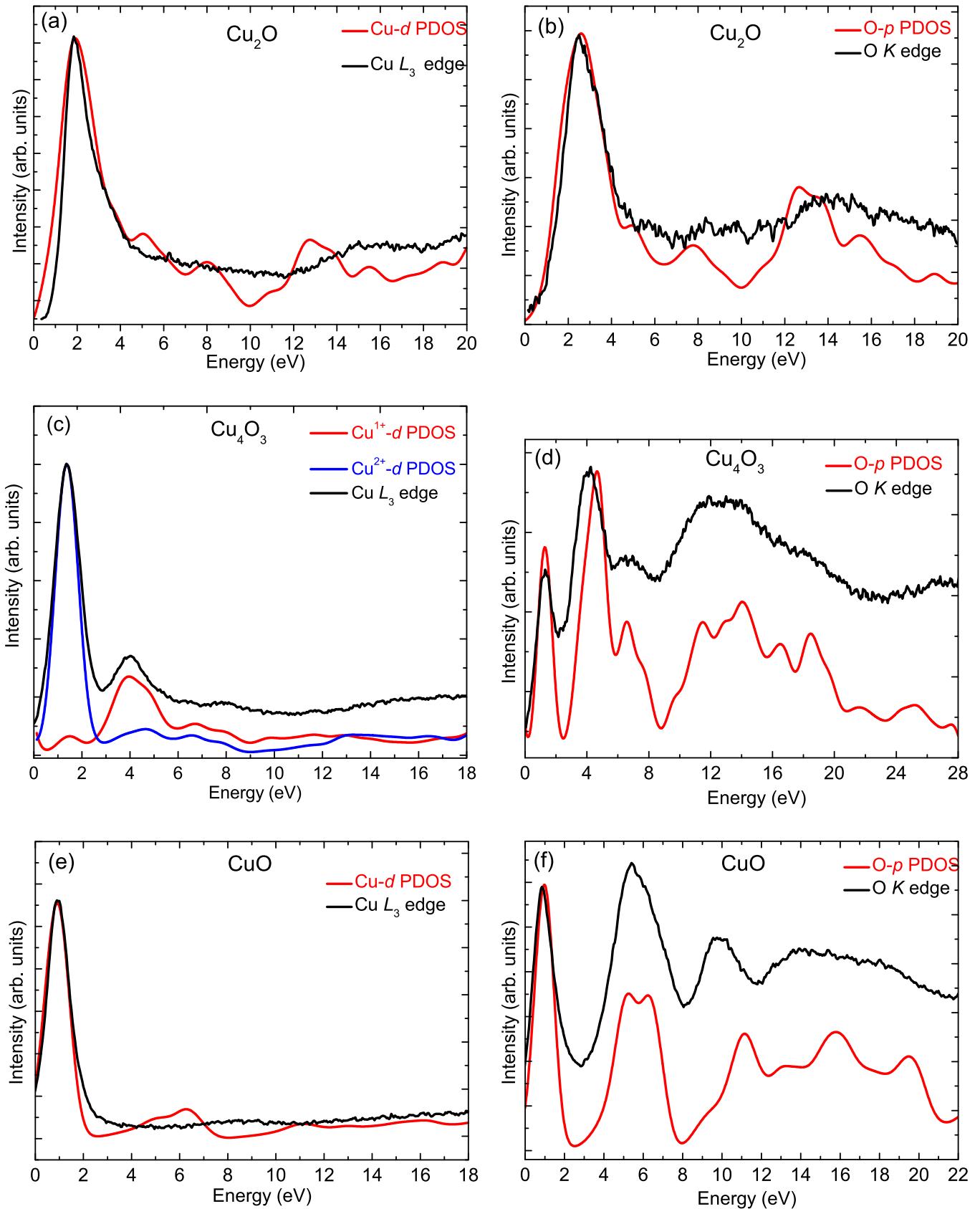


FIG. 6. The comparison between experimental Cu L_3 edge ELNES spectrum and Cu- d PDOS in conduction band for (a) Cu₂O, (c) Cu₄O₃, and (e) CuO. The comparison between experimental O K edge ELNES spectrum and O- p PDOS in conduction band for Cu₂O, Cu₄O₃, and CuO is displayed in (b), (d), and (f), respectively. The experimental spectra are shifted to align with the leading peak of PDOS.

Cu₄O₃, respectively, based on the comparison with the *GW* calculations. Similarly, the features in the O *K* spectrum are well described by the PDOS up to energies of about 20 eV above the conduction band minimum (CBM) [Fig. 6(d)].

The comparisons for CuO are shown in Figs. 6(e) and 6(f), which demonstrates that also here most of the experimental features are well reproduced by the theory, even though some minor differences are observed, e.g. the peak at about 4 eV in O *K* edge of Cu₄O₃ has a shift with theoretical position [see Fig. 6(d)], or the peak at 6 eV in Cu-*d* PDOS of CuO is not clearly observed in the experiments [see Fig. 6(e)]. Such differences could well result from the simple PDOS model that does not fully account for the optical transition matrix element and for the energy dependence of the electron-core hole interaction.

IV. CONCLUSIONS

A joint experimental and theoretical study has been carried out to investigate the electronic structures of Cu₂O, Cu₄O₃, and CuO thin films. Optical absorption, photoemission, and EELSs have been employed to determine the band gap, valence, and conduction band structures, respectively, which are compared with theoretical results from many-body *GW* calculations employing an additional onsite potential for the Cu-*d* orbital energies. Applying this approach to the less studied oxide Cu₄O₃, we predict an indirect band gap of 0.84 eV and a direct band gap of 1.59 eV. For CuO, we obtain an indirect band gap of 1.24 eV and a direct band gap of 1.46 eV. The consistency between the calculated and measured absorption spectra corroborates the prediction of indirect band gaps in these Cu²⁺ containing oxides.

XPS and UPS have been combined together to study the valence band structure. In combination with the theoretical electronic structure results, a consistent picture was obtained where the Cu-*d* photoemission peaks of Cu²⁺ and Cu¹⁺ lie around -4 and -3 eV relative to the VBM, respectively, across all three oxides. Fully accounting for hybridization effects and band dispersion, the *GW* calculations reveal that the O-*p* DOS straddles the DOS peak of the Cu-*d*⁹ manifold. Thus, CuO cannot be unambiguously described as either Mott or charge transfer insulator, but has features of both. An important finding for the interpretation of photoemission data is that CuO and Cu₄O₃ seem to be subject to surface reduction

under vacuum conditions, leading to the attenuation of the Cu²⁺ peak at -4 eV and to a shift of the apparent peak position between XPS and UPS. As a result of the surface reduction, the photoemission spectra of CuO and Cu₄O₃ are hardly distinguishable.

The comparative study across the three Cu oxides benefited greatly from the application of EELS, which resolves the rich structure of electronic structure features in the conduction band. Since EELS is much less surface sensitive, it offered a significant advantage over XPS to distinguish the three phases in the Cu *L*_{2,3} edges or O *K* edge spectra. The predicted PDOS in the conduction band agrees remarkably well with the EELS spectra, providing further confidence in the computational description of the overall electronic structure.

Notwithstanding the use of the *V*_d onsite potential, which acts as a simple potential offset of equal magnitude for all three oxides, it is remarkable that the *GW* method provides a consistent electronic structure picture across both correlated Mott/charge-transfer insulators (CuO, Cu₄O₃) and band insulators (Cu₂O). This is not possible, for example, in hybrid functional calculations without a specific parameter adjustment. This finding strongly suggests that electron correlation effects are rather well captured in *GW*. Thus, addressing current technical limitations, such as the quality of input wave functions, the convergence of RPA response functions, and vertex corrections, will likely enable fully parameter-free predictions of band structures and optical properties in correlated materials.

ACKNOWLEDGMENTS

Y.W. would like to acknowledge the European Commission for the Erasmus Mundus Ph.D. fellowship with the DocMASE project. Y.W. would like to thank Dr. Simon Karl Moser (Ecole Polytechnique Fédérale de Lausanne), Dr. Junfeng Han (Beijing University of Science and Technology), and Alexis Molter (Université de Lorraine) for fruitful discussion. F.S. and F.M. would like to thank the Europäische Fonds für Regionale Entwicklung (EFRE) Funds of the European Commission for support of activities within the AME-Lab project. S.L. was supported by the US Department of Energy, Office of Science, Office of Basic Energy Sciences, as part of an Energy Frontier Research Center under Contract No. DE-AC36-08GO28308 to National Renewable Energy Laboratory (NREL).

-
- [1] T. Kazimierzczuk, D. Fröhlich, S. Scheel, H. Stolz, and M. Bayer, *Nature* **514**, 343 (2014).
 - [2] A. Zakutayev, V. Stevanovic, and S. Lany, *Appl. Phys. Lett.* **106**, 123903 (2015).
 - [3] Y. S. Lee, D. Chua, R. E. Brandt, S. C. Siah, J. V. Li, J. P. Mailoa, S. W. Lee, R. G. Gordon, and T. Buonassisi, *Adv. Mater.* **26**, 4704 (2014).
 - [4] B. K. Meyer, A. Polity, D. Reppin, M. Becker, P. Hering, P. J. Klar, T. Sander, C. Reindl, J. Benz, M. Eickhoff, C. Heiliger, M. Heinemann, J. Bläsing, A. Krost, S. Shokovets, C. Müller, and C. Ronning, *Phys. Status Solidi B* **249**, 1487 (2012).
 - [5] Y. Ievskaya, R. L. Z. Hoye, A. Sadhanala, K. P. Musselman, and J. L. MacManus-Driscoll, *Sol. Energy Mater. Sol. Cells* **135**, 43 (2014).
 - [6] T. Minami, Y. Nishi, and T. Miyata, *Appl. Phys. Lett.* **105**, 212104 (2014).
 - [7] B. Pecquenard, F. Le Cras, D. Poinot, O. Sicardy, and J. P. Manaud, *ACS Appl. Mater. Interfaces* **6**, 3413 (2014).
 - [8] A. Y. Anderson, Y. Bouhadana, H. N. Barad, B. Kupfer, E. Rosh-Hodesh, H. Aviv, Y. R. Tischler, S. Rühle, and A. Zaban, *ACS Comb. Sci.* **16**, 53 (2014).

- [9] J. Ghijsen, L. H. Tjeng, J. van Elp, H. Eskes, J. Westerink, G. A. Sawatzky, and M. T. Czyzyk, *Phys. Rev. B* **38**, 11322 (1988).
- [10] X. G. Zheng, C. N. Xu, Y. Tomokiyo, E. Tanaka, H. Yamada, and Y. Soejima, *Phys. Rev. Lett.* **85**, 5170 (2000).
- [11] M. Grioni, J. F. van Acker, M. T. Czyzyk, and J. C. Fuggle, *Phys. Rev. B* **45**, 3309 (1992).
- [12] F. P. Koffyberg and F. A. Benko, *J. Appl. Phys.* **53**, 1173 (1982).
- [13] P. Jiang, D. Prendergast, F. Borondics, S. Porsgaard, L. Giovanetti, E. Pach, J. Newberg, H. Bluhm, F. Besenbacher, and M. Salmeron, *J. Chem. Phys.* **138**, 024707 (2013).
- [14] J. F. Pierson, A. Thobor-Keck, and A. Billard, *Appl. Surf. Sci.* **210**, 359 (2003).
- [15] F. Marabelli, G. B. Parravicini, and F. Salghetti-Drioli, *Phys. Rev. B* **52**, 1433 (1995).
- [16] M. Heinemann, B. Eifert, and C. Heiliger, *Phys. Rev. B* **87**, 115111 (2013).
- [17] S. Lany, *Phys. Rev. B* **87**, 085112 (2013).
- [18] L. Y. Isseroff and E. A. Carter, *Phys. Rev. B* **85**, 235142 (2012).
- [19] A. Soon, X. Y. Cui, B. Delley, S. H. Wei, and C. Stampfl, *Phys. Rev. B* **79**, 035205 (2009).
- [20] H. Raebiger, S. Lany, and A. Zunger, *Phys. Rev. B* **76**, 045209 (2007).
- [21] C. Rödl, F. Sottile, and L. Reining, *Phys. Rev. B* **91**, 045102 (2015).
- [22] J. P. Hu, D. J. Payne, R. G. Egdell, P.-A. Glans, T. Learmonth, K. E. Smith, J. Guo, and N. M. Harrison, *Phys. Rev. B* **77**, 155115 (2008).
- [23] Y. Wang, J. Ghanbaja, F. Soldera, S. Migot, P. Boulet, D. Horwat, F. Mücklich, and J. F. Pierson, *Appl. Surf. Sci.* **335**, 85 (2015).
- [24] L. Debbichi, M. C. Marco de Lucas, and P. Krüger, *Mater. Chem. Phys.* **148**, 293 (2014).
- [25] J. F. Pierson, E. Duverger, and O. Banakh, *J. Solid State Chem.* **180**, 968 (2007).
- [26] K. B. Grun, M. Sieskind, and S. Nikitine, *J. Phys. Chem. Solids* **19**, 189 (1961).
- [27] A. Daunois, J. L. Deiss, and B. Meyer, *J. Phys. (Paris)* **27**, 142 (1966).
- [28] Q. Zhang, K. Zhang, D. Xu, G. Yang, H. Huang, F. Nie, C. Liu, and S. Yang, *Prog. Mater. Sci.* **60**, 208 (2014).
- [29] C. E. Ekuma, V. I. Anisimov, and M. Jarrell, *Eur. Phys. J. B* **87**, 23 (2014).
- [30] B. J. Hansen, N. Kouklin, G. Lu, I. K. Lin, J. Chen, and X. Zhang, *J. Phys. Chem. C* **114**, 2440 (2010).
- [31] D. Wu, Q. Zhang, and M. Tao, *Phys. Rev. B* **73**, 235206 (2006).
- [32] R. F. Egerton, *Electron Energy-Loss Spectroscopy* (Springer, New York, 2011).
- [33] C. Rödl, F. Fuchs, J. Furthmüller, and F. Bechstedt, *Phys. Rev. B* **79**, 235114 (2009).
- [34] S. V. Faleev, M. van Schilfgaarde, and T. Kotani, *Phys. Rev. Lett.* **93**, 126406 (2004).
- [35] F. Bruneval, N. Vast, L. Reining, M. Izquierdo, F. Sirotti, and N. Barrett, *Phys. Rev. Lett.* **97**, 267601 (2006).
- [36] S. Lany, *J. Phys. Condens. Matter* **27**, 283203 (2015).
- [37] Y. Wang, J. Ghanbaja, F. Soldera, P. Boulet, D. Horwat, F. Mücklich, and J. F. Pierson, *Acta Mater.* **76**, 207 (2014).
- [38] Y. Wang, P. Miska, D. Pilloud, D. Horwat, F. Mücklich, and J. F. Pierson, *J. Appl. Phys.* **115**, 073505 (2014).
- [39] L. Hedin, *Phys. Rev.* **139**, A796 (1965).
- [40] G. Kresse and D. Joubert, *Phys. Rev. B* **59**, 1758 (1999).
- [41] M. Shishkin and G. Kresse, *Phys. Rev. B* **74**, 035101 (2006).
- [42] J. B. Forsyth, P. J. Brown, and B. M. Wanklyn, *J. Phys. C Solid State Phys.* **21**, 2917 (1988).
- [43] J. P. Perdew, K. Burke, and M. Ernzerhof, *Phys. Rev. Lett.* **77**, 3865 (1996).
- [44] S. L. Dudarev, G. A. Botton, S. Y. Savrasov, C. J. Humphreys, and A. P. Sutton, *Phys. Rev. B* **57**, 1505 (1998).
- [45] J. Paier, M. Marsman, and G. Kresse, *Phys. Rev. B* **78**, 121201(R) (2008).
- [46] J. Klimeš, M. Kaltak, and G. Kresse, *Phys. Rev. B* **90**, 075125 (2014).
- [47] M. Shishkin, M. Marsman, and G. Kresse, *Phys. Rev. Lett.* **99**, 246403 (2007).
- [48] A. Gruneis, G. Kresse, Y. Hinuma, and F. Oba, *Phys. Rev. Lett.* **112**, 096401 (2014).
- [49] H. Peng and S. Lany, *Phys. Rev. B* **87**, 174113 (2013).
- [50] T. A. Pascal, U. Boesenberg, R. Kostecki, T. J. Richardson, T.-C. Weng, D. Sokaras, D. Nordlund, E. McDermott, A. Moewes, J. Cabana, and D. Prendergast, *J. Chem. Phys.* **140**, 034107 (2014).
- [51] R. W. Nunes and X. Gonze, *Phys. Rev. B* **63**, 155107 (2001).
- [52] K. J. Blobaum, D. Van Heerden, A. J. Wagner, D. H. Fairbrother, and T. P. Weihs, *J. Mater. Res.* **18**, 1535 (2003).
- [53] V. Stevanovic, S. Lany, X. Zhang, and A. Zunger, *Phys. Rev. B* **85**, 115104 (2012).
- [54] A. Jolk and C. F. Klingshirn, *Phys. Status Solidi B* **206**, 841 (1998).
- [55] See Supplemental Material at <http://link.aps.org/supplemental/10.1103/PhysRevB.94.245418> for [brief description].
- [56] J. J. Yeh and I. Lindau, *At. Data Nucl. Data Tables* **32**, 1 (1985).
- [57] Z. X. Shen, R. S. List, D. S. Dessau, F. Parmigiani, A. J. Arko, R. Bartlett, B. O. Wells, I. Lindau, and W. E. Spicer, *Phys. Rev. B* **42**, 8081 (1990).
- [58] M. R. Thuler, R. L. Benbow, and Z. Hurych, *Phys. Rev. B* **26**, 669 (1982).
- [59] M. Finazzi, G. Ghiringhelli, O. Tjernberg, Ph. Ohresser, and N. B. Brookes, *Phys. Rev. B* **61**, 4629 (2000).
- [60] A. R. Williams and N. D. Lang, *Phys. Rev. Lett.* **40**, 954 (1978).
- [61] M. Grioni, J. B. Goedkoop, R. Schoorl, F. M. F. de Groot, J. C. Fuggle, F. Schäfers, E. E. Koch, G. Rossi, J.-M. Esteva, and R. C. Karnatak, *Phys. Rev. B* **39**, 1541 (1989).
- [62] H. Tan, J. Verbeeck, A. Abakumov, and G. Van Tendeloo, *Ultramicroscopy* **116**, 24 (2012).